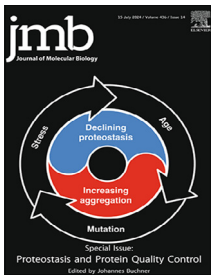

Epigenetic Histone Modifications H3K36me3 and H4K5/8/12/16ac Induce Open Polynucleosome Conformations via Different Mechanisms

Yi-Yun Lin [1,2], Peter Müller [1,2], Evdoxia Karagianni [2], Nicola Hepp [3,4], Felix Mueller-Planitz [3], Willem Vanderlinden [1,2,5,*] and Jan Lipfert [1,2,*]

*1 - **Department of Physics and Center for NanoScience (CeNS),** LMU Munich, Amaliensstrasse 54, 80799 Munich, Germany*
*2 - **Soft Condensed Matter and Biophysics,** Department of Physics and Debye Institute for Nanomaterials Science, Utrecht University, Princetonplein 1, 3584 CC Utrecht, the Netherlands*
*3 - **Institute of Physiological Chemistry,** Faculty of Medicine Carl Gustav Carus, Technische Universität Dresden, Fetscherstraße 74, 01307 Dresden, Germany*
*4 - **Current address: Department of Clinical Genetics,** Rigshospitalet, Copenhagen University Hospital, Blegdamsvej 9, 2100 Copenhagen, Denmark*
*5 - **School of Physics and Astronomy,** University of Edinburg, James Clerk Maxwell Building, Peter Guthrie Tait Road, Edinburgh EH9 3FD, United Kingdom*

Correspondence to Willem Vanderlinden and Jan Lipfert: Department of Physics and Center for NanoScience (CeNS), LMU Munich, Amaliensstrasse 54, 80799 Munich, Germany. *Willem.Vanderlinden@ed.ac.uk (W. Vanderlinden), J.Lipfert@uu.nl (J. Lipfert)*
https://doi.org/10.1016/j.jmb.2024.168671
Edited by Sepideh Khorasanizadeh

Abstract

Nucleosomes are the basic compaction unit of chromatin and nucleosome structure and their higher-order assemblies regulate genome accessibility. Many post-translational modifications alter nucleosome dynamics, nucleosome-nucleosome interactions, and ultimately chromatin structure and gene expression. Here, we investigate the role of two post-translational modifications associated with actively transcribed regions, H3K36me3 and H4K5/8/12/16ac, in the contexts of tri-nucleosome arrays that provide a tractable model system for quantitative single-molecule analysis, while enabling us to probe nucleosome-nucleosome interactions. Direct visualization by AFM imaging reveals that H3K36me3 and H4K5/8/12/16ac nucleosomes adopt significantly more open and loose conformations than unmodified nucleosomes. Similarly, magnetic tweezers force spectroscopy shows a reduction in DNA outer turn wrapping and nucleosome-nucleosome interactions for the modified nucleosomes. The results suggest that for H3K36me3 the increased breathing and outer DNA turn unwrapping seen in mononucleosomes propagates to more open conformations in nucleosome arrays. In contrast, the even more open structures of H4K5/8/12/16ac nucleosome arrays do not appear to derive from the dynamics of the constituent mononucleosomes, but are driven by reduced nucleosome-nucleosome interactions, suggesting that stacking interactions can overrule DNA breathing of individual nucleosomes. We anticipate that our methodology will be broadly applicable to reveal the influence of other post-translational modifications and to observe the activity of nucleosome remodelers.

Introduction

Nucleosomes are the basic building block of eukaryotic genomes, essential for the organization, compaction, and regulation of genetic information.[1–3] Canonical nucleosome core particles are composed of two copies of H2A, H2B, H3, and H4 assembled into a histone octamer that is wrapped by 147 bp of DNA[2,4] (Figure 1A). Interaction within nucleosomes stems from both electrostatic interactions and specific molecular contacts.[5–9] The nucleosome core interacts with adjacent nucleosomes to form the higher order structure, so that, ultimately, the genomic DNA on a scale of ~1 m can be packed and condensed into the nucleus, which is on a scale of ≈10 μm.[10–16] However, the DNA must remain accessible for various cellular processes such as replication, transcription, and repair.[17–21] Multiple factors affect the compaction and chromatin structure to regulate those cellular processes. Epigenetic modifications, or post-translational modification (PTMs), a diverse array of covalent chemical marks that modulate gene expression without altering the DNA sequence, have emerged as critical regulators of chromatin architecture and function.[22–26] In eukaryotic cells, histones are subject to hundreds of PTMs including acetylation, methylation, ubiquitination, phosphorylation, and sumoylation.[27] Histones PTMs are widely distributed throughout the whole genome. They can control the accessibility of DNA or recruit chromatin remodelers to regulate gene expression.[22–26,28–30] Histone PTMs are present both in the tails of histones and their globular core domains.[31,32] By introducing additional charge, neutralizing existing charge, or by adding steric constraints, different modifications affect the compaction of chromatin and also modulate the stability of nucleosomes. In particular, methylation and acetylation have been intensively studied as marks of chromatin status involving active or silenced transcription.[25,27] For acetylation ("ac"), histone acetylation neutralizes the positive charge of lysine, which reduces interactions with DNA and has been shown to e.g., enable transcription factor binding within nucleosomes.[33–35] Acetylation of H4 tail has a strong effect on weakening chromatin packing *in vivo* and *in vitro*.[33,36–38] H3 acetylation also reduces the charge of the tails but the effect on folding propensity of nucleosome arrays is less clear.[35,39]

Histone methylation ("me") occurs on the side chains of lysines or arginines[40] and, unlike acetylation, does not alter the charge of histone protein and is thought to act mainly via "reader" enzymes that specifically recognize the methylated site and then activate or repress transcription.[41] For example, H3K9 and H3K27 methylation are often related to silenced chromatin states.[41] Examples of chromatin readers that recognize methylation and are involved in gene repression are HP1 that binds to H3K9me3 and contributes to heterochromatin formation[42,43] and the methyltransferase PRC2 that acts on H3K27[44] and recruits other accessory protein to propagate the H3K27me3 mark resulting in gene silencing.[45–47] In contrast, H3K36 methylation is associated with actively transcribed regions.[48,49] Importantly, H3K36me3 acts as a binding hub for chromatin readers featuring chromo-, PWWP, or Tudor domains.[50–52]

While traditional biochemical and structural methods have provided valuable insights into nucleosome architecture, these approaches often entail ensemble measurements that obscure the intrinsic heterogeneity and dynamic nature of these macromolecular assemblies. Recently, single-molecule techniques have provided an ability to probe nucleosomes at the level of individual molecules.[53–57] In particular, AFM imaging has been used to visualize the structure and dynamics of nucleosomes and their interactions.[58–66] We have recently developed a high-throughput pipeline to image individual nucleosomes[60,62] and applied the approach to determine the effect of several epigenetic modifications on mononucleosome conformational landscape. AFM imaging of mononucleosomes revealed that H3K36me3 nucleosomes are, on average, more open and wrap less DNA, while H3S10 phosphorylation and H4K5/8/12/16ac did not significantly affect conformations of individual nucleosomes.[61] A complementary approach has been to probe nucleosomes and nucleosome arrays by force spectroscopy, in optical[67–70] and magnetic tweezers,[55,71] which enable to apply forces and monitor the resulting changes in extension.[55,69,71,72] Force-spectroscopy approaches have revealed changes in extension in intermediate nucleosome conformations and characterized the folding of chromatin fibers and higher order assemblies.[55,69–71,73,74]

Here, we go beyond mononucleosomes and probe the effect of epigenetic modifications on nucleosome-nucleosome interactions using arrays with three nucleosomes, where the conformational landscape of individual nucleosomes is modulated and constrained by interactions. We complement our AFM imaging results using magnetic tweezers force-spectroscopy measurements.[75–80] By applying mechanical forces and observing the ensuing responses, we can probe nucleosome conformations and interactions and go beyond the static structures revealed by AFM imaging.[58–62,81] To be able to directly compare to previous work on mononucleosomes, we again contrast unmodified with the H3K36me3 and H4K5/8/12/16ac modifications. This choice enables us to probe nucleosomes under conditions where H1 linker histones are not expected to play an important role[82] and to contrast the role of enhanced intrinsic breathing (which has been shown[61] to be the case for H3K36me3) and inter-nucleosome stacking interactions (which we expect[33,83–85] for H4K5/8/12/16ac). Our single-

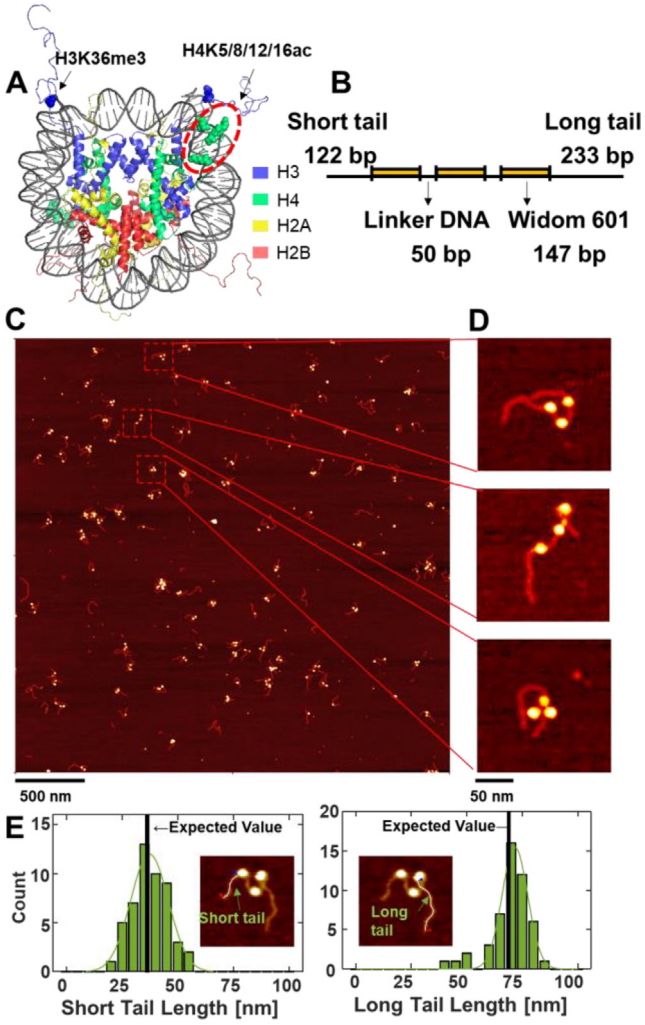

Figure 1. Analysis of tri-nucleosome conformations by AFM imaging. (A) Crystal structure of a canonical nucleosome (PDB 1KX5). Colored spheres represent the positions of the modified amino acids in the histone tail. Residues involve in H3K36me3 (i.e. three additional methyl groups at lysine 36 of histone H3) shown as a blue sphere and in H4K5/8/12/16 ac (i.e. acetylation of H4 histones at lysines 5, 8, 12 and 16) as green spheres. **(B)** Schematic of the DNA construct used for AFM imaging. The 896 bp DNA consists of three 147 bp Widom 601 nucleosome positioning sequences that are flanked by a short and a long arm of 122 bp and 233 bp, respectively. **(C)** AFM image of DNA and tri-nucleosome sample with a field of view of 3 μm × 3 μm (recorded with 2048 × 2048 pixels). **(D)** Zooms of selected tri-nucleosomes in the AFM image in panel C. **(E)** Histograms of short and long arm length of unmodified tri-nucleosomes (N = 49 molecules analyzed), with a Gaussian fitted to each distribution (green solid line). Insets show example image of tri-nucleosomes with the poly-line profile indicated that was used to measure the arm lengths. Vertical lines are the expected arm length computed from the number of base pairs in the short and long arm, respectively, and assuming 0.314 ± 0.013 nm/bp.

molecule results consistently indicate that both H3K36me3 and H4K5/8/12/16ac lead to more open conformations in the context of tri-nucleosome constructs, by reducing stacking interactions and increasing nucleosome breathing.

Results and Discussion

Assembly and AFM imaging of tri-nucleosome arrays

To prepare nucleosome samples for AFM imaging, we assembled different variant nucleosomes by salt gradient dialysis on 896 bp DNA constructs. Our DNA construct features three Widom 601 (W601) sequences[86] partitioned by 50 bp of linker DNA and flanked by a short arm 122 bp and long arm 233bp (Figure 1B and Materials and Methods). The same DNA construct was used for the different nucleosome variants. We deposited nucleosome samples on poly-L-lysine coated mica and recorded high-resolution AFM images (see Materials and Methods for details). AFM images (Figure 1C) are obtained by amplitude modulation AFM in air and further analyzed to dissect the influences of PTMs on structural

dynamics and geometry. The AFM images show populations of naked DNA, mono-, di-, and tri-nucleosomes (Supplementary Figure 1). We designed the DNA construct with two different length arms flanking the region with the W601 sequences to be able to determine nucleosome positioning. To quantify the positioning, we first evaluate the length of the two arms for individual tri-nucleosome particles (see Materials and Methods for details) (Figure 1D, E). The length of the short arm and long arm are 37.3 ± 8.4 nm and 71.6 ± 6.4 nm, respectively. These results are in an excellent agreement with the expected values of 38 nm and 73 nm for short and long arm, assuming a DNA length per base pair of 3.14 ± 0.13 Å found previously by AFM imaging under similar conditions,[60] fully consistent with positioning of the nucleosomes on the W601 sequences.

We use AFM imaging to confirm the assembly of different variant nucleosomes and quantify the different polynucleosome populations, by counting the number of mono-, di-, tri-, and even occasional tetra-nucleosomes (requiring nucleosome loading to DNA outside of the W601 sequences) that are successfully assembled (Supplementary Figure 1). The populations for bare DNA, and DNA with one, two, three, and four nucleosomes are consistent, within experimental errors, with a simple binomial distribution (Supplementary Figure 1), which implies that the assembly of the different variant nucleosomes on the three W601 sites are all relatively uncooperative under the conditions of our experiments, consistent with previous observations.[81,87] We find similar probabilities P for sites being occupied for the different variants, with nearly identical values for unmodified (P = 0.418 ± 0.010) and H4K5/8/12/16ac (P = 0.415 ± 0.008). H3K36me3 exhibits a slightly lower occupation probability of P = 0.344 ± 0.008, which might be due to minor differences in the protein concentration due to experimental variability or due to a slightly lower affinity of the tri-methylated variant. Overall, AFM imaging confirms that nucleosomes of all three variants are assembled robustly on our DNA construct, with similar affinities and relatively low cooperativity between positing sites.

AFM imaging reveals conformational changes of tri-nucleosome arrays induced by epigenetic modifications

To study the effect of selected PTMs on nucleosome structure, we analyze the configuration of tri-nucleosomes by extracting several structure parameters from AFM images. In a first step, we use process images in SPIP and identify the tri-nucleosome samples (Supplementary Figure 2). Nucleosome positions are ordered from the nucleosome closest to the short tail to the one closest to long tail (referred to as N_1, N_2, N_3) and we extract the x and y positions of the nucleosome centers (Supplementary Figure 2). We then compute three different geometrical parameters to quantify tri-nucleosome conformations. First, we determine the radius of gyration defined by $R_g = \left(\frac{d1^2+d2^2+d3^2}{3}\right)^{\frac{1}{2}}$, where ($d1$, $d2$, $d3$) are the distances from the nucleosome positions to their center of mass (Supplementary Figure 2C). Second, we calculate the distance between the first nucleosome and the third, which we call the N_1N_3-distance. Third, we compute the inner angle α, defined as the angle between the lines connecting N_2 to N_1 and N_3, using the formula $\alpha = \cos^{-1}\left(\frac{a \cdot b}{|a| \cdot |b|}\right)$ with a and b are two dimensional vectors of the nucleosome particles (Supplementary Figure 2D, $\vec{a} = \vec{N_2N_1}$, $\vec{b} = \vec{N_2N_3}$).

We compare the distributions of the geometric parameters obtained by AFM imaging for the different nucleosome species in our study to quantify the impact of the different PTMs (Figure 2 and Supplementary Figure 3). We find that the radii of gyration, N_1N_3-distances, and inner angles provide a highly consistent picture: The unmodified nucleosomes adopt the most compact conformations, exhibiting narrow distributions, with the smallest mean values for all three parameters. Conversely, H4K5/8/12/16ac nucleosomes present the broadest range and largest average values, while H3K36me3 nucleosomes have distributions for radii of gyration, N_1N_3-distances, and inner angles that are intermediate between the other two nucleosome types (Table 1 and Figure 2). Together, these data suggest that H4K5/8/12/16ac nucleosomes exhibit the least compact and most open conformations, while unmodified nucleosomes exhibit the most compact structures and H3K36me3 nucleosomes take on intermediate conformations. For each type of nucleosome, we prepared two independent reconstitutions that were each measured in at least 6 independent AFM experiments. We find consistent distributions of parameters across the independently prepared reconstitutions suggesting that our analysis is robust (Supplementary Figure 4). Consequently, we pooled all data for each nucleosome type for the subsequent analyses.

To make the pairwise comparisons quantitative and to test whether the observed differences are statistically significant, we perform four different analyses, separately for all three conformational parameters (i.e. for radii of gyration, N_1N_3-distances, and inner angles): (i) we compare the full distributions using Kolmogorov-Smirnov tests (a non-parametric test for the equality of 1-dimensional probability distributions), (ii) we compare the means of the distributions using two-sample t-tests and alternative, (iii) two-sample Z-tests, and (iv) we compare the fraction of conformations that are particular open using manually selected threshold values using two-sample proportion tests (Figure 2, Supplementary Table 1, and Supplementary Figure 3).

Table 1 Mean value and standard deviation (SD) of three parameter: Radius of gyration (Rg), N_1N_3-Distance (N_1N_3), and inner angle (Angle) from Figure 2.

	Unmodified	H3K36me3	H4K5/8/12/16ac
Number of tri-nucleosomes	495	460	549
Mean Rg (nm)	14.2	16.0	16.6
SD Rg (nm)	4.2	6.0	5.4
Mean N_1N_3 (nm)	24.8	29.0	32.4
SD N_1N_3 (nm)	12.6	16.3	15.3
Mean Angle (°)	66.3	71.7	83.5
SD Angle (°)	41.8	46.0	46.5

Using Kolmogorov–Smirnov tests to compare the full distribution of R_g, N_1-N_3-distance, and inner angle α between the different variant nucleosomes (Figure 2, black brackets, and Supplementary Table 1), we find statistically significant differences for all parameters (R_g, N_1N_3-distance, and inner angle) and for each pairwise comparison, except for the inner angle comparison between unmodified and H3K36me3. Comparing the mean values for radii of gyration, N_1N_3-distances, and inner angles, we find statistically significant differences with unmodified nucleosomes being most compact and H4K5/8/12/16ac taking on the largest values, except for the radii of gyrations comparison between H3K36me3 and H4K5/8/12/16ac and the inner angle comparison between unmodified and K3K36me3, which are not significant (Figure 2, grey brackets, and Supplementary Table 1). We find essentially identical significance levels from two-sample *t*-tests and *Z*-tests.

In addition to comparing the overall distributions and their means, we look at the subpopulations with open conformations, defined as having R_g, N_1-N_3-distance, or inner angle values above manually determined thresholds (Supplementary Figure 3M–O). The thresholds were selected to exclude the main peak at low values for R_g, N_1-N_3-distance, or inner angle values and to quantify the fraction of molecules in particular open conformations. The fraction of tri-nucleosomes occupying particularly open structures increases, in almost all cases statistically significantly, in going from unmodified, to H3K36me3, and further to H4K5/8/12/16ac nucleosomes, further confirming the observations from the overall distributions and mean values (Supplementary Table 1 and Supplementary Figure 3).

The more open configurations for H3K36me3 compared to unmodified tri-nucleosome arrays are in line with the behavior of the constituent mononucleosomes. Previous work using a high-throughput AFM analysis approach to probe mononucleosomes found that H3K36me3 mononucleosomes have increased breathing activity, are almost 2-fold less likely to occupy the fully wrapped state and exhibit less anti-cooperativity for unwrapping from the respective ends compared to unmodified nucleosomes.[61] In contrast, the same assay found no difference between the conformations of H4K5/8/12/16ac and unmodified mononucleosomes, in stark contrast to our findings for tri-nucleosomes.

To directly compare how mononucleosome conformations vary across the different PTMs under the conditions of our assay, we exploit the fact that in our tri-nucleosome samples there is a sub-population of molecules with only one nucleosome assembled (Supplementary Figure 1). We analyzed this sub-population of mononucleosomes by tracing the DNA entry/exit angles using the tangent method, wherein the angle is measured by drawing tangents along the two DNA arms in proximity of the nucleosome core (Supplementary Figure 5). From the analysis of the mononucleosome sub-population in our tri-nucleosome measurements, we find that H3K36me3 nucleosomes have statistically significant larger mean exit angles compared to unmodified and H4K5/8/12/16ac nucleosomes, while there is no significant difference between the unmodified and H4K5/8/12/16ac condition (Supplementary Figure 5), in excellent agreement with the previous analysis using mononucleosome samples assembled on shorter DNA with only one W601 positioning sequence.[61] Therefore, we conclude that increased nucleosome breathing constitutes a mechanism underlying the more open tri-nucleosome configurations in H3K36me3 versus unmodified nucleosomes, whereas the mechanism underlying de-compaction of H4K5/8/12/16ac nucleosomes must be different.

Next, we assessed whether the overall compaction of nucleosomes also governs the local accessibility of nucleosomal DNA in the context of trinucleosomes. To this end, we measured the entry/exit angle of DNA for the central nucleosome in trinucleosomes using the tangent method. The *DNA entry/exit angle* correlates linearly with the extent of DNA wrapped,[60] and is not necessarily equivalent to the *inner angle* defined above (which is the angle formed by connecting the centers of trincleosome cores) because the linker DNA connecting the constituting nucleosomes can be significantly bent (Supplementary Figure 6).

We find that the DNA entry/exit angles for unmodified and H3K36me3 mononucleosomes (mean angles of 97 ± 3° and 106 ± 3°, respectively; error is SEM, Supplementary Figure 5) are larger than the DNA entry/exit angles of the middle nucleosome in tri-nucleosomes (mean angles of 86 ± 4° and 95 ± 4°; error is SEM, Supplementary Figures 6 and 7). In contrast, for H4K5/8/12/16ac the mean DNA entry/exit angle for mononucleosomes is 90 ± 4° (error is SEM, Supplementary Figure 5) and the mean DNA entry/exit angle for the central nucleosome in tri-nucleosomes is 104 ± 5° (error is SEM, Supplementary Figure 6). A plausible explanation is that for unmodified and H3K36me3 nucleosomes, nucleosome-nucleosome interactions restrict the opening and conformational space of the central nucleosome in the context of tri-nucleosomes significantly. Nevertheless, it is important to note that intrinsic tendencies of nucleosome unwrapping are preserved in the context of nucleosome assemblies and possibly in larger nucleosome arrays. The larger DNA inner opening angle of H4K5/8/12/16ac variant in trinucleosomes as compared to mononucleosomes, could tentatively be explained by steric effects, where the bulk of neighboring nucleosomes drives unwrapping.

Together, the observations suggest that the acetylation of H4K5/8/12/16ac nucleosomes primarily affects nucleosome-nucleosome interactions and the open, more dynamic conformations of H4K5/8/12/16ac tri-nucleosome mostly occur due to a decrease in stacking and/or binding interactions between the nucleosomes, compared to unmodified and H3K36me3. Our experimental observations for H4K5/8/12/16ac tri-nucleosomes are in good agreement with molecular simulations that investigated histone tail acetylation dependence of the free energy landscape of tri-nucleosome and found that tri-nucleosomes with H4 acetylation have a larger R_g compared to unmodified nucleosomes and also reduce the contact between first and third nucleosomes mediated by the histone tails.[84] Our results support that H4-acetylation opens nucleosome array by reducing the inter-nucleosome interaction.[85]

Effect of the ion atmosphere on tri-nucleosome conformations

Since chromatin structure is sensitive to the ionic environment,[60,88–93] we performed control AFM imaging measurement using a different buffer composition and compared the structural parameter in the presence of different types of salt. It is well-known that Mg^{2+} can affect the compaction of chromatin.[88,91,94,95] Mg^{2+} can help chromatin to turn from 'beads-on-a-string' into a 30 nm fiber *in vitro*[94] and Mg^{2+} and K^+ mixed environment seems important for the structure of heterochromatin formation.[96] Previous work by sedimentation velocity analytical ultracentrifugation on nucleosome arrays in different mixed salt solution shows that the additions of Mg^{2+} leads to the precipitation of nucleosome arrays in solution with KCl or NaCl.[90] Therefore, we compared the condition with mixed cations Mg^{2+} and K^+ (2 mM $MgCl_2$ and 100 mM KCl; which is approximately the physiological concentration of ions intracellularly[97–99]) that was used for the data described above to a buffer comprising 200 mM NaCl and no Mg^{2+}, which has similar ionic strength compared to the mixed ion condition and is the buffer used previously for AFM imaging of mononucleosomes.

The results show that both unmodified tri-nucleosome and the acetylated tri-nucleosome adopt more compact structures in the presence of Mg^{2+} and K^+ (Supplementary Figure 8), in line with previously observed trends for chromatin. However, the effect of the change in ionic conditions is smaller than the effect of the PTMs on structure. In fact, the change induced by changing from the NaCl imaging buffer to the mixed conditions with Mg^{2+} was smaller, for all parameters analyzed, than the difference between unmodified and H4K5/8/12/16ac nucleosomes (Supplementary Figure 8). In conclusion, while we find that the addition of Mg^{2+} compacts tri-nucleosome arrays in agreement with previous findings, the observed influence of PTMs on the structure of tri-nucleosome is similar for different salt conditions and dominates under the conditions employed here and we, therefore, focus on the role of PTMs.

Magnetic tweezers force spectroscopy probes unmodified, H4K5/8/12/16ac, and H3K36me3 tri-nucleosome constructs

Having established that H3K36me3 and H4K5/8/12/16ac influence internucleosome interactions and result in more open polynucleosome structures, we asked how the PTMs affect the properties of the tri-nucleosomes in a dynamic setting by using multiplexed magnetic tweezers. To study the behavior of variant nucleosomes under controlled stretching forces, we assembled nucleosomes on a 2823 bp DNA construct with biotin labels on one and DBCO labels at the other end, separated by unmodified DNA from a central segment containing three W601 and 50 bp of linker DNA each (Figure 3A). To produce sufficient DNA for *in vitro* nucleosome reconstitution and with appropriate labels for stable attachment in the tweezers, we used our megaprimer approach described previously[87] and reconstituted unmodified, H3K36me3, and H4K5/8/12/16 tri-nucleosomes on the construct (Materials and Methods and Supplementary Figure 9). The biotin labels enable attachment to streptavidin-coated magnetic beads (M270, 2.7 μm diameter), while the DBCO labeled-end provides covalent attachment to an

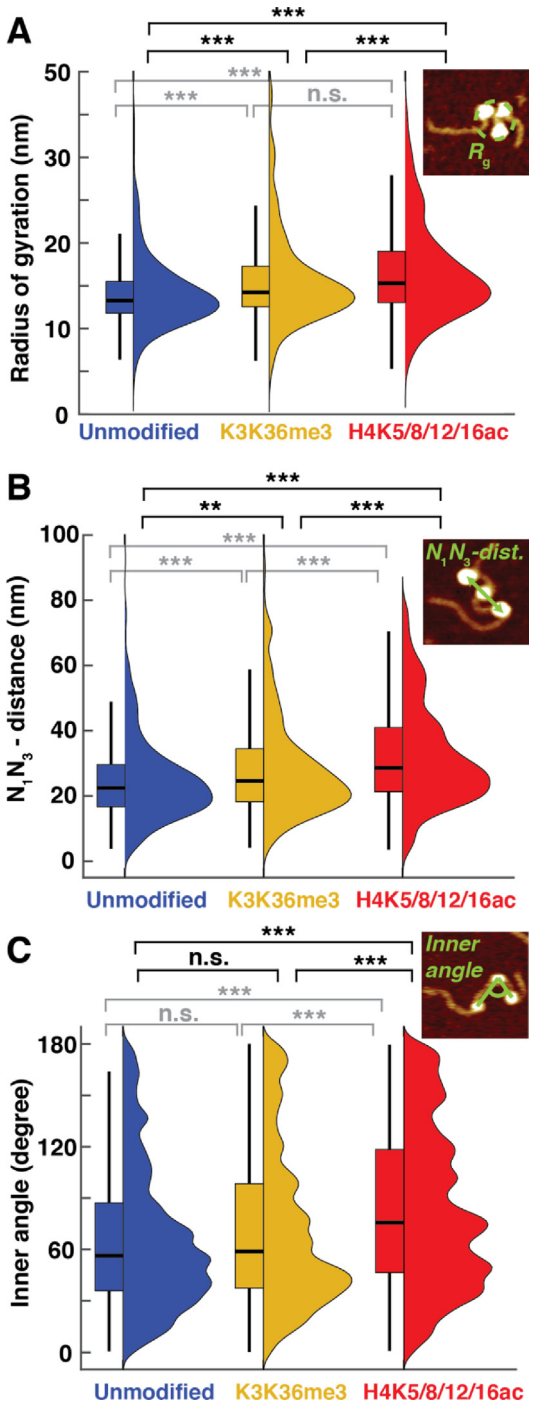

Figure 2. AFM imaging reveals the impact of H3K36me3 and H4K5/8/12/16ac PTMs on tri-nucleosome conformations. (A–C) Probability distributions for radii of gyration (A), N_1N_3-distances (B), and inner angles (C) determined from AFM imaging for unmodified ($N = 495$ tri-nucleosome arrays), H3K36me3 ($N = 460$), and H4K5/8/12/16ac ($N = 549$) nucleosomes. The insets show example images of the corresponding tri-nucleosomes (unmodified top, H3K36me3 middle, H4K5/8/12/16ac bottom) and illustrate the geometrical parameters analyzed. Data are shown as violin plots on the right and as boxplots of the left. The central bar in the boxplots indicates the median, the box the 25th and 75th percentile. Whiskers indicate the full range after excluding outliers that are beyond 1.5 times the interquartile range of the 25th and 75th percentile, respectively. Black bars and symbols indicate significant differences between the distributions based on the results of two-sample Kolmogorov-Smirnov (KS) tests; Gray bars and symbols above the boxplots indicate significant differences between the means based on two-sample two-tailed *t*-tests: n.s. not significant, $*p < 0.05$, $**p < 0.01$, $***p < 0.001$. Using two-sample *Z*-tests gives the same levels of significance as indicated for the *t*-tests. An overview with all *p*-values from statistical tests is given in Supplementary Table 1. Additional analyses and representations of the same data are shown in Supplementary Figure 3.

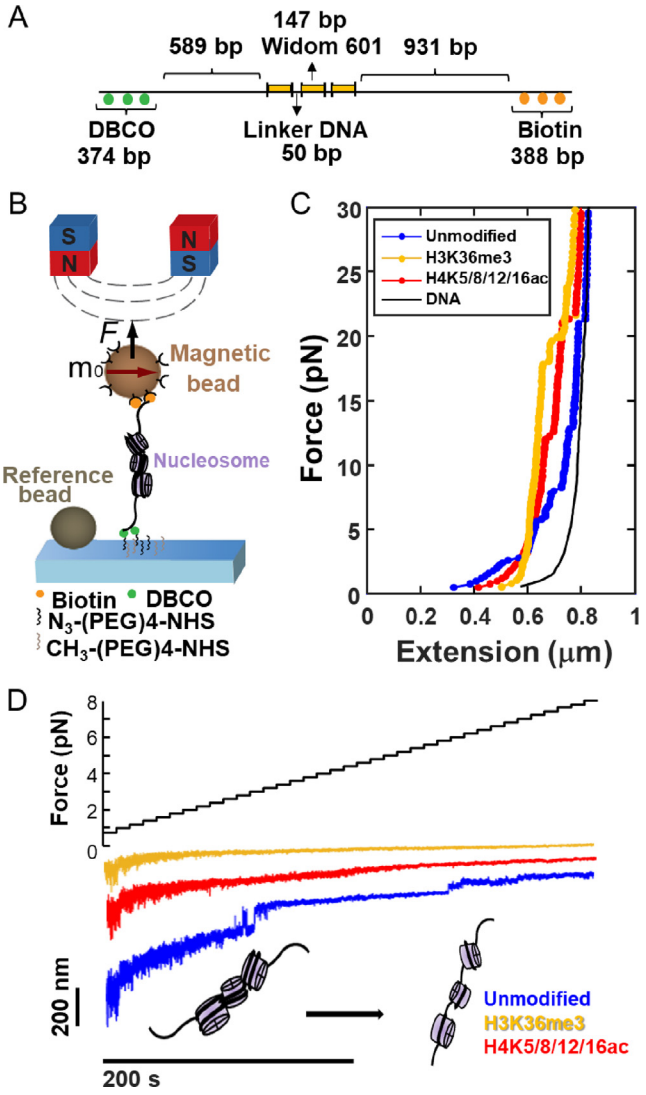

Figure 3. Probing tri-nucleosomes in magnetic tweezers. (A) Schematic of the DNA construct used for magnetic tweezers. The 2823 bp DNA consists of three 147 bp Widom 601 nucleosome positioning sequences that are flanked by a 589 bp short arm and extra 374 bp fragment with DBCO labeled, and a 931 bp long arm and extra 388 bp fragment with biotin labeled, respectively. **(B)** Schematic of the magnetic tweezer set-up. Nucleosomes are reconstituted on DNA with two functionalized ends, one labeled with multiple biotins and the other with multiple DBCOs. The DNA construct is amplified by using the ligation free "megaprimer" method described previously.[87] The flow cell surface is functionalized with azide-$(PEG)_4$-NHS. The magnetic beads are labeled with streptavidin. **(C)** Force-extension curves of different variant nucleosomes and bare DNA anchored as shown in panel A. Nucleosome samples were stretched under applied forces from 0.5 to 30 pN. **(D)** Force ramp at low force (Force $\leq$ 8 pN; top) of different variants of nucleosome. The extension time traces (color curves; bottom) show different length plateaus at forces $\leq$ 8 pN that indicate outer turn unwrapping and unstacking of polynucleosomes. Same color code as in panel C.

azide-functionalized glass slide surface via copper-free click chemistry[87] (Figure 3A). To confirm the assembly of nucleosomes and to quantify the different polynucleosome populations, we again used AFM imaging to count the number of successfully assembled mono-, di-, tri-nucleosomes (Supplementary Figure 10). The distributions show similar binomial distributions as we observed for the assembly on shorter length DNA used for AFM analysis discussed above.

We performed force-extension experiments on polynucleosome arrays by applying constant forces in the magnetic tweezers from 0.5 to 30 pN in 0.2 pN increments, each for 5 s (for forces > 8 pN) or 10 s ($\leq$8 pN). Extension traces are obtained by subtracting the position of a surface attached reference bead from the magnetic bead positions[79,80] and our instrument achieves high spatio-temporal resolution and excellent stability (Material and Methods and Supplementary Fig-

ure 11). The raw extension traces reveal considerable variability for all variant polynucleosomes (Figure 3C and Supplementary Figure 12), showing the heterogeneity and complexity of our reconstituted samples, in line with our AFM imaging results. The time traces also reveal that, superimposed on the expected force-extension stretching response of double-stranded DNA, there are jumps and hopping events visible in the data, qualitatively in line with nucleosomes unwrapping and unstacking. We compare the different tri-nucleosome constructs by taking the mean extension for each force plateau to obtain force-extension curves (Figure 3B). We find that at low forces ($\leq$8 pN), the unmodified nucleosome tethers tend to have a shorter extension compared to H3K36me3 and H4K5/8/12/16ac. In addition, the raw extension vs. time traces below for forces $\leq$8 pN show that unmodified nucleosomes exhibit larger fluctuations due to hopping or stepping contributions compared to H3K36me3 and H4K5/8/12/16ac constructs (Figure 3C and Supplementary Figure 12). At high forces (>8 pN) all types of nucleosomes show steps with comparable properties.

Repeated stretching and release cycles indicate that mechanical forces disrupt some but not all nucleosome interactions

We observe clear differences in the tether responses between the first stretching cycle (going from 0.5 to 30 pN) and the first release or second stretching cycle (Supplementary Figure 13). After the first stretching cycle, the tether lengths at a given force are increased compared to the initial stretching cycle for all nucleosome variants investigated, suggesting that at least some of the nucleosome structures are permanently disrupted by applying forces, in agreement with previous literature.[67,100] Nonetheless, repeated force-extension cycles still show steps and a decreased extension, compared to bare DNA, at low forces, implying that some nucleosomes remain bound or can rebind even after stretching to 30 pN, consistent with previous observations that the core particle may reassemble upon relaxation after peeling off the inner turn DNA.[56,67,69,101,102]

Force spectroscopy suggests a reduction of stacking and outer turn wrapping interactions in H4K5/8/12/16ac and H3K36me3 compared to unmodified nucleosomes

The time traces in the low force regime ($\leq$8 pN) exhibit a broad range of steps, hopping behavior, and gradual changes in extension, while the traces at higher forces show more clearly defined steps. We attribute the changes in the range of 2–8 pN to unwrapping of the outer turn of DNA from nucleosomes and the disruption of nucleosome-nucleosome interactions. In contrast, the defined steps at high forces (>8 pN) agree with previous reports[55,56,71,72,100,103–109] of non-equilibrium peeling of the inner ~75 bp of DNA from the core of the octamer. Here, we first discuss the behavior at low forces ($\leq$8 pN) and in the next section we analyze the steps at higher forces.

To compare the different variant nucleosomes in force-extension measurements, we compute the mean extension in z for each force plateau and calculate the difference in z between adjacent force steps (Figure 4A), which we define as Δz. Spikes in Δz correspond to abrupt jumps in tether lengths (Figure 4B). The computed Δz values show that all types of nucleosomes demonstrate multiple spikes from low to high forces (Figure 4B). Unmodified nucleosomes have a higher density of spikes, and the spikes are distributed over a broader range of forces. For both H3K36me3 and H4K5/8/12/16ac, the spikes are less dense at low force regime ($\leq$8 pN) compared to the unmodified condition. We analyze the Δz distribution at forces ranging from 2 to 8 pN (Figure 4C). The result shows statistically significant differences between all types of nucleosomes and also between the different nucleosomes and bare DNA (except for H3K36me3), as assed by two-sample Kolmogorov-Smirnov tests (Figure 4C and Supplementary Table 2). The H3K36me3 and H4K5/8/12/16ac nucleosomes have narrower Δz distributions with lower means (Figure 4C), statistically significantly different from unmodified nucleosomes, but not from each other, as assessed by two-sample *t*-tests (Figure 4C and Supplementary Table 2). The reduced number of larger stepping events in the force range 2–8 pN for H3K36me3 and H4K5/8/12/16ac compared to unmodified tri-nucleosomes suggests that these PTMs disrupt nucleosome-nucleosome stacking and outer turn wrapping. The magnetic tweezers observations are in line with AFM results that indicate more open conformations for H3K36me3 and H4K5/8/12/16ac. The gradual disruption of stacking and wrapping interactions is expected to give rise to differences between subsequent force plateaus beyond those seen for bare DNA and, therefore, to an increase in the observed Δz populations, as is clearly observed for unmodified nucleosomes. Conversely, of wrapping or stacking interactions are disrupted and conformations are already relatively open at low forces, we expect smaller Δz values, as is observed for H3K36me3 and H4K5/8/12/16ac nucleosomes.

Interestingly, while the AFM results suggest that H4K5/8/12/16ac tri-nucleosomes adopt the most open conformations, the magnetic tweezers measurements see the smallest mean Δz population for H3K36me3. However, we note that the difference in mean Δz steps sizes between H3K36me3 and H4K5/8/12/16ac is within experimental error.

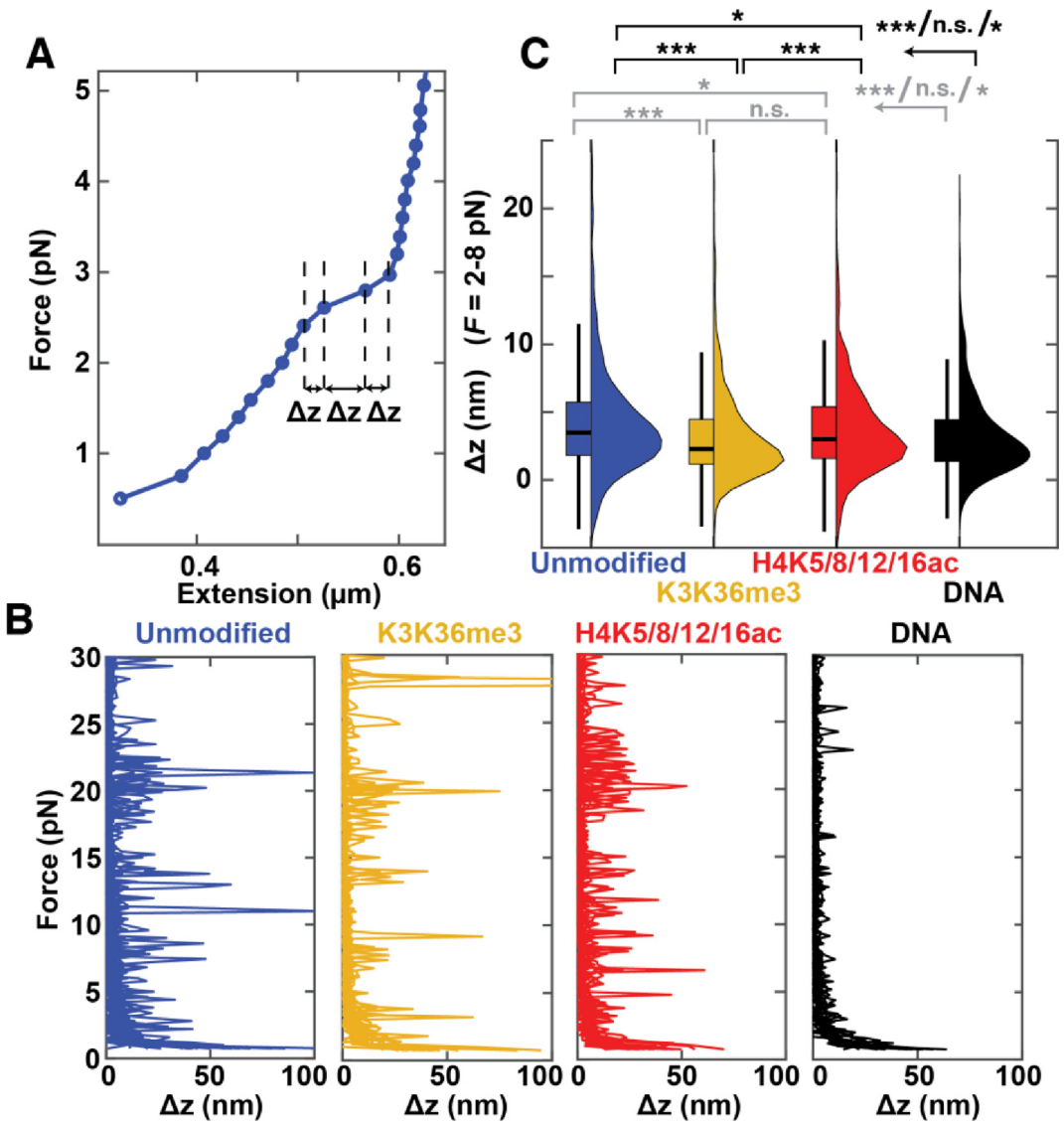

Figure 4. Analysis of force-extension reveals nucleosome unstacking and unwrapping. (A) Schematic of the Δz analysis, using (part of) the unmodified nucleosome force-extension curve from Figure 3B. We analyzed the force-extension data for polynucleosomes by averaging each force plateau's extension *z* and subtracting the average *z* from the previous force plateau to obtain Δz. **(B)** Δz vs. force data for unmodified ($N = 20$), H3K36me3 ($N = 16$), H4K5/8/12/16 ($N = 17$), and DNA ($N = 15$) nucleosomes. **(C)** Distributions of the Δz values using the data in the force range 2–8 pN for different variant nucleosomes and bare DNA. Data are shown as violin plots on the right and as boxplots of the left. The central bar in the boxplots indicates the median, the box the 25th and 75th percentile. Whiskers indicate the full range after excluding outliers that are beyond 1.5 times the interquartile range of the 25th and 75th percentile, respectively. Black bars and symbols indicate significant differences between the distributions based on the results of two-sample Kolmogorov-Smirnov (KS) tests; Gray bars and symbols above the boxplots indicate significant differences between the means based on two-sample two-tailed *t*-tests: n.s. not significant, $*p < 0.05$, $**p < 0.01$, $***p < 0.001$. The annotation for the bare "DNA" condition indicates the pairwise comparisons to the three different types of nucleosomes, respectively. An overview with all p-values from the different statistical tests is given in Supplementary Table 2.

Force spectroscopy finds no influence of the investigated PTMs on inner turn unwrapping of nucleosomes

The Δz vs. force plots from variant nucleosomes also show that at higher forces (>8 pN), there are multiple spikes regardless of nucleosome types (Figure 4B). The corresponding steps are consistent with inner turn nucleosome unwrapping. To quantify the effects of the investigated PTMs on inner turn unwrapping, we analyzed the extension steps at high forces (>8 pN) with the step finding algorithm by Kerssemakers *et al.*[110] to identify unwrapping

steps in our extension vs. time traces (Figure 5A). From the fits, we determine the differences of average extensions before and after the steps to obtain step sizes. The distributions of step sizes from the three different types of nucleosomes show very similar peaks with mean step sizes between 22–26 nm (Figure 5B), in excellent agreement with previous reports for step sizes of inner turn unmodified nucleosome unwrapping in the range of 20–30 nm [55,56,71,72,100,103–109]. In addition, we analyze the forces at which the high-force steps occur to quantify the force range of inner turn unwrapping. We again find remarkably similar force distributions for all types of nucleosomes studied, with mean forces well within experimental error, at 17–19 pN (Figure 5C). The results suggest that the H3K36me3 and H4K5/8/12/16ac PTMs have no significant effects on inner turn nucleosome disassembly. Inner turn nucleosome unwrapping is sudden due to the strong interactions near to positions ± 40 bp of DNA from the dyad axis.[111] Overall, the interactions between the inner turn DNA wrap and the histone octamer involve both electrostatic and non-electrostatic interactions, while the outer DNA wrap interactions with the histone octamer are dominated by electrostatic interactions.[104,111] Consequently, the changes at the N-tail due to H4K5/8/12/16ac or H3K36me3 are unlikely to affect the inner turn nucleosomal DNA unwrapping, consistent with our experimental findings.

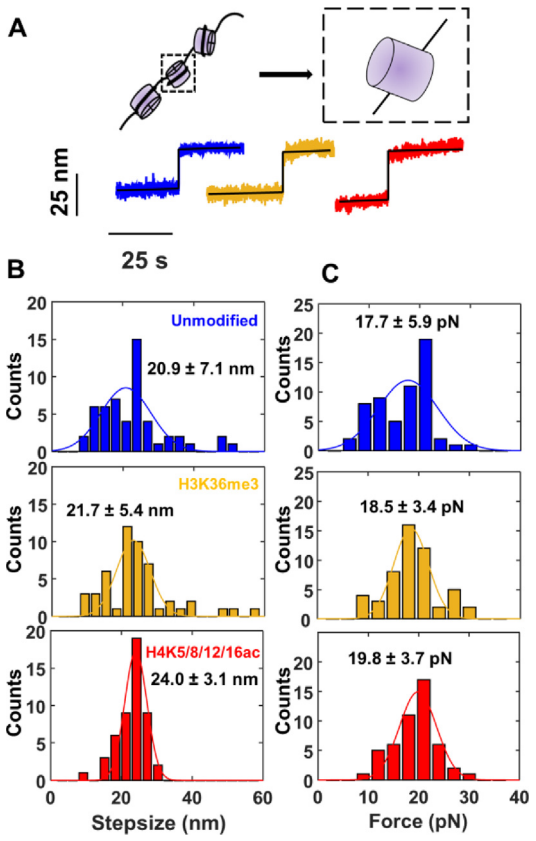

Figure 5. Analysis of inner turn DNA unwrapping in tri-nucleosome constructs under force. (A) Example of a discrete steps in time traces (colored data) at forces >8 pN, characteristic of the unwrapping of the inner DNA turn from nucleosomes. Black lines are fitted steps using algorithm by Kerssemakers *et al.*[110] Unmodified nucleosome, blue line; H3K36me3 nucleosome, yellow line; and H4K5/8/12/16ac nulceosome, red line. **(B)** Histograms of the step sizes for inner turn unwrapping as determined in panel A. Solid lines are Gaussian fits and the means are indicated in the panels. **(C)** Histogram of the forces for inner turn unwrapping corresponding to the steps in panel B. Solid lines are Gaussian fits and the means and standard deviations are indicated in the panels. The step sizes and forces are not significantly different for any of the pairwise comparisons as determined by two-sample *t*-tests.

Conclusion

PTMs are a key factor that affects the structure and dynamics of chromatin fibers in the cell. They can have manifold effects on chromatin structure, such as entry site unwrapping, nucleosome destabilization, formation of active or repressive compartments, and histone-histone destabilization.[31,32,112] Here we investigate the conformations of post-translational modified nucleosomes using two single-molecule techniques: atomic force microscopy imaging and magnetic tweezer force spectroscopy. Specifically, we study the effects of the post-translational modifications H3K36me3 and H4K5/8/12/16ac on tri-nucleosome array structure and mechanical stability. We use tri-nucleosomes, which has been reported to be the smallest cluster size found in cells,[113] as a tractable model system for comparison of different PTMs on nucleosome arrays that build in complexity on our previous work on mononucleosomes in isolation.[61]

H3K36me3 and H4K5/8/12/16ac are known as markers of active region in chromatin. Previous high-throughput AFM image analysis has shown that H3K36me3 mononucleosomes exhibit partial unwrapping and more open conformations compared to unmodified mononucleosomes, likely due to the position of the H3K36me3 mark at the DNA entry/exit site of the nucleosome.[29,92] We confirmed this finding by analyzing the mononucleosome sub-population of our tri-nucleosome samples and find significantly higher exit angles for H3K36me3 nucleosomes compared to unmodified and H4K5/8/12/16ac species (Supplementary Figure 5). It has been found that PTMs at the entry/exit region enhance partial DNA unwrapping.[31,61,114] Our results here suggest that the increased unwrapping induced by the H3K36me3 seen in mononucleosomes propagates to higher order nucleosome assemblies, as we observe more open and loose conformations for H3K36me3 compared to unmodified nucleosomes both by AFM imaging magnetic and tweezers force spec-

troscopy. Our findings are in line with previous simulations that predict nucleosome breathing to affect their higher order structures, to result in more heterogeneous nucleosome-nucleosome contacts.[115]

The H3K36me3 modification is associated with DNA repair, alternative splicing, and transcription. It is enriched in the region of actively transcribed genes[50,116,117] and serves as an interaction hub for chromatin readers.[50–52] Our finding that H3K36me3 leads to more open nucleosome array structures highlights a mechanism how it can facilitate access of histone-binding proteins, e.g. of protein carrying a PWWP domain[118] that interact with the H3K36me3 mark and regulate gene transcription.[50,117]

Interestingly, the H4K5/8/12/16ac modification causes no significant changes in mononucleosome structure compared to unmodified mononucleosome,[61] yet it leads to the most open and extended tri-nucleosome structures as judged by the AFM imaging results, of the three variants studied. This is consistent with the view that the H4K5/8/12/16ac mark, which is known to be associated with open chromatin conformations,[33,119] reduces nucleosome-nucleosome interactions and stacking. The fact that H4K5/8/12/16ac tri-nucleosomes are more open and less compact than the H3K36me3 constructs suggests that nucleosome-nucleosome interactions can be more important and overrule nucleosome breathing and outer turn unwrapping.

In vitro work reveals that H4K5/8/12/16ac inhibits liquid–liquid phase separation, likely due to the decrease of multivalent interaction with other nucleosomes.[120] Our experiments are consistent with this observation of reduced liquid–liquid phase separation by H4K5/8/12/16ac nucleosomes, as our observations imply reduced nucleosome-nucleosome interactions. In contrast, the inner turn unwrapping appears to not be influenced by the investigated PTMs, consistent with the view that their influence is limited to the entry-exit site and tail regions.

Chromatin architecture is more open at transcriptionally active sites.[121] Here we demonstrate that epigenetic marks associated with active transcription can decrease chromatin compaction directly – not only by reducing nucleosome-nucleosome interactions but also by outer turn wrapping affinity. Taken together, our work suggests that the combination of force spectroscopy and AFM imaging can provide a comprehensive understanding of how different PTMs affect nucleosome assemblies and we anticipate our approach to be powerful to study the effect of other PTMs, and their interplay with chromatin readers, in the future.

Materials and Methods

DNA preparation

We created the plasmid pFMP218 containing three repeats of a 197 bp Widom-601 nucleosome positioning sequence as follows. A pUC18-based plasmid containing 25 consecutive repeats of a 197 bp Widom 601 nucleosome positioning sequence with an AvaI restriction site in each linker (pFMP166; kind gift from D. Rhodes, NTU, Singapore) was completely digested with AvaI. The monomeric 197 bp long Widom 601 DNA and the vector backbone were gel purified. Monomeric DNA was ligated back into the pUC18-based vector backbone. One colony harbored a trimeric 601 repeat as revealed by an analytical digest with EcoRI and HindIII. The correct sequence was confirmed by Sanger sequencing.

We then used the plasmid pFMP218 as template to produce DNA constructs with 3 repeats of the Widom 601 sequence for the AFM and MT measurements, respectively. The DNA construct for AFM measurements has a length of 896 bp. We prepared the DNA by PCR with Phusion Hot Start polymerase (follow the vendor's protocol) by using forward primer 5′-TAAGTTGGGTAACGC CAGG-3′ and reverse primer 5′-GGCCGATTCAT TAATGCAGC-3′ (Supplementary Figure 14). The final PCR product was purified with the QIAquick PCR Purification Kit (Qiagen).

The functionalized DNA constructs used for MT measurement were prepared using our recently developed "megaprimer" approach.[87] In brief, the method is based on first preparing two ≈380 bp functionalized DNA strands that are assembled in separate PCR reactions with 40–50% biotin-16-dUTP or 40–50% DBCO-$(PEG)_4$-dUTP replacement for dTTP, respectively. The two functionalized DNAs are then used as primers (or "megaprimers") in a second PCR reaction step to amplify the final 2823 bp DNA. The final DNA construct consequently has DBCO and biotin labels, respectively, at the two opposite ends (Supplementary Figure 9), enabling covalent attachment to the bottom surface of the magnetic tweezers flow cell via DBCO-based copper-free click chemistry and to the streptavidin-coated magnetic beads via the biotin labels (see "DNA or polynucleosome anchoring for magnetic tweezers experiments" below). The PCR products were purified with the QIAquick PCR Purification Kit (Qiagen) after each step of PCR amplification. Details of the megaprimer protocol, including concentrations, sequences, and PCR parameters are described in Lin et al.[87] An advantage of the approach is that it enables straightforward assembly of functionalized DNA constructs in sufficient quantities to enable nucleosome reconstitution.

Nucleosome reconstitution

Nucleosomes were assembled on the labeled DNA construct obtained using the megaprimer protocol outlined in the previous section. Unmodified and modified histone proteins were purchased from EpiCypher (Durham, North Carolina). We followed the previously published

protocol to prepare nucleosome reconstitutions.[87] Nucleosome reconstitutions were performed by salt gradient dialysis. The preparation of nucleosome samples for AFM measurement and MT measurement, respectively, used dialysis chambers containing 2.8–3 μg of the 896 bp DNA or the 2823 bp megaprimer DNA with biotin and DBCO labels and different histone octamers (ratio of histone octamer to Widom 601 is 1 to 1.5) at 2 M NaCl that were placed in 300 ml high-salt buffer (2 M NaCl, 10 mM Tris, 1 mM EDTA). 3 L of low-salt buffer (50 mM NaCl, 10 mM Tris, 1 mM EDTA) were transferred to the high-salt buffer at 4 °C overnight.

AFM sample preparation, imaging, and analysis

We followed the previously published protocols to prepare samples for AFM imaging.[60–62,122,123] The reconstituted nucleosomes were incubated in 100 mM KCl, 2 mM $MgCl_2$, and 10 mM Tris–HCl, pH 7.6, for 1 min on ice and then deposited on poly-L-lysine (0.01% w/v) coated muscovite mica for 30 s, followed by 20 ml Milli-Q water rinsing and drying with a gentle stream of filtered N_2 gas. AFM imaging was performed on a Nanowizard Ultraspeed 2 (JPK, Berlin,Germany) with AFM cantilevers 240AC-NA (Opus) in air. All AFM images were acquired in tapping mode at room temperature. The scans were recorded at 1 Hz line frequency over a field of view of 3 μm × 3 μm at 2048 × 2048 pixels. For image processing, Scanning Probe Image Processor (SPIP v6.5.1; Image Metrology) was employed. Image processing involved background correction by using global fitting with a third-order polynomial and line-by-line correction through the histogram alignment routine.

Mononucleosomes were then selected for DNA exit angle analysis according to the tangent method (see Supplementary Figure 5). For trinucleosomes, we used the particle analysis toolbox in SPIP to obtain the (x,y) center coordinates of the individual constituting nucleosomes. These center coordinates are then used to calculate the radius of gyration, the N1-N3 distance, and the angle of the inner nucleosome with respect to the outer nucleosomes N1 and N3 (see Figure 2). In addition, we used the tangent method to evaluate the DNA exit angle of the inner nucleosome N2 in trinucleosomes (see Supplementary Figure 6).

AFM measurements presented in this work, in particular the data in Figure 2, are based on at least two independent nucleosome reconstitutions measured using at least 6 independent surface depositions for each type of nucleosome. We observed good agreement between the different batches from independent reconstitutions for the same type of nucleosome (Supplementary Figure 4).

Magnetic tweezers setup

We used a custom-built MT setup described previously.[124] The setup was equipped with a pair of 5 × 5 × 5 mm^3 permanent magnets (W-05-N50-G, Supermagnete, Switzerland) with a 1 mm gap in vertical configuration.[125] In the setup, a DC-motor (M-126.PD2, Physik Instrumente, Germany) controls the distance between magnets and the flow cell. A LED (69647, Lumitronix LED Technik GmbH, Germany) was used for illumination. In addition, a 40× oil-immersion objective (UPLFLN 40x, Olympus, Japan) and a CMOS sensor camera with 4096 × 3072 pixels (12 M Falcon2, Teledyne Daisa, Canada) were utilized to image a field of view of 400 × 300 μm^2. Images were recorded at 58 Hz and transferred to a frame grabber (PCIe 1433; National Instruments, Austin TX). By tracking images in real-time with custom-written tracking software (Labview, National Instruments), we can extract the (x,y,z) coordinates of all beads.[126,127] The objective is mounted on a piezo stage (Pifoc P726. 1CD, PI Physikinstrumente) to build a look-up table (LUT) for tracking the bead z-position. With a step size of 100 nm, the LUT was generated over a range of 10 μm. Set up control and bead tracking used Labview routines described previously.[126]

Flow cell assembly and preparation

Flow cells were assembled from two microscope cover slips with a parafilm spacer. The bottom coverslip (24 × 60 mm, Carl Roth, Germany) was treated with 2% APTES to generate an aminosilanized surface. Before flow cell assembly, 5000x diluted stock solution of polystyrene beads with 1 μm diameter (Polysciences, USA) in ethanol (Carl Roth, Germany) was deposited on the amino-coated coverslip and then slowly dried. These immobile surface-bound beads serve as reference beads for drift correction, which enables high-resolution measurements with excellent stability. We quantify the spatio-temporal resolution by Allan deviations analysis[128–131] and find a tracking accuracy frame-to-frame of ≈1–2 nm and excellent stability over measurement times >30 min (Supplementary Figure 11). The bottom coverslip was aligned with a pre-cut parafilm and a top coverslip with two small holes for inlet and outlet. Then the assembled flow cell was baked at 80 °C for 1 min to create a seal.

DNA or polynucleosome anchoring for magnetic tweezers experiments

DNA or polynucleosome anchoring was carried out as described.[87] Briefly, following flow cell assembly, 50 mM each of azide-$(PEG)_4$-NHS (Jena Biosciences GmbH, Jena, Germany) and methyl-$(PEG)_4$-NHS (Life technologies) in 1 × PBS were introduced and incubated for 1 h.[132] We mixed our DNA or polynucleosome sample in measurement

buffer MB1 (MB1; 10 mM HEPES pH 7.6, 100 mM KCl, 2 mM $MgCl_2$, 0.1% Tween-20). Next, DNA or polynucleosome were dissolved in 100 μl MB1, flushed into the flow cell and incubated for 1 h. Afterwards, we rinsed with MB2 buffer, which consists of MB1 supplemented with 0.1% (w/v) bovine serum albumin (Carl Roth, Germany) to flush away unbound nucleosome or DNA. Subsequently, we flowed in 1% casein for nucleosome samples or 1.5% (w/v) bovine serum albumin for DNA samples in MB2 into the flow cell, incubated for 1 h to minimize nonspecific interactions. Finally, we flushed in streptavidin-coated M270 beads (Dynabeads, Invitrogen) and incubated with samples to form tethers. After flushing away free magnetic beads with several cell volumes of MB2, we start the measurements. MT data, in particular the data in Figure 4, are based on at least 6 independent repeat measurements.

CRediT authorship contribution statement

Yi-Yun Lin: Writing – original draft, Visualization, Project administration, Investigation, Formal analysis, Conceptualization. **Peter Müller:** Visualization, Investigation, Formal analysis. **Evdoxia Karagianni:** Investigation, Formal analysis. **Nicola Hepp:** Investigation. **Felix Mueller-Planitz:** Supervision, Writing – review & editing. **Willem Vanderlinden:** Writing – review & editing, Visualization, Supervision, Project administration, Conceptualization. **Jan Lipfert:** Writing – review & editing, Supervision, Project administration, Funding acquisition, Conceptualization.

DATA AVAILABILITY

Data will be made available on request.

DECLARATION OF COMPETING INTEREST

The authors declare that they have no known competing financial interests or personal relationships that could have appeared to influence the work reported in this paper.

Acknowledgements

We thank Thomas Nicolaus, Dave van den Heuvel, Relinde van Dijk-Moes, and Elleke van Harten for laboratory assistance, Lori van de Cauter, Sebastian Konrad, Tine Brouns, and Philipp Korber for useful discussions, Stefanie D. Pritzl, Ivo Vermaire and Diogo Saraiva for support with measurements, and Friedrich Förster, Louris Feitsma, Joke Granneman, Mariska Gröllers-Mulderij, and the entire Structural Biochemistry group at Utrecht University for useful discussion and laboratory use.

Funding

This work was supported by the Deutsche Forschungsgemeinschaft (DFG, German Research Foundation) through SFB 863, Project 111166240 A11, Utrecht University, and MU 3613/1-285.

Appendix A. Supplementary material

Supplementary material to this article can be found online at https://doi.org/10.1016/j.jmb.2024.168671.

Received 18 February 2024;
Accepted 16 June 2024;
Available online 20 June 2024

Keywords:
nucleosomes;
chromatin;
methylation;
acetylation;
single-molecule methods

References

1. Khorasanizadeh, S., (2004). The nucleosome: from genomic organization to genomic regulation. *Cell* **116**, 259–272.
2. Kornberg, R.D., (1974). Chromatin structure: a repeating unit of histones and DNA. *Science* **184**, 868–871.
3. Hewish, D.R., Burgoyne, L.A., (1973). Chromatin substructure. The digestion of chromatin DNA at regularly spaced sites by a nuclear deoxyribonuclease. *Biochem. Biophys. Res. Commun.* **52**, 504–510.
4. Richmond, T.J., Davey, C.A., (2003). The structure of DNA in the nucleosome core. *Nature* **423**, 145–150.
5. Davey, C.A., Sargent, D.F., Luger, K., Maeder, A.W., Richmond, T.J., (2002). Solvent mediated interactions in the structure of the nucleosome core particle at 1.9 a resolution. *J. Mol. Biol.* **319**, 1097–1113.
6. Luger, K., Mader, A.W., Richmond, R.K., Sargent, D.F., Richmond, T.J., (1997). Crystal structure of the nucleosome core particle at 2.8 A resolution. *Nature* **389**, 251–260.
7. McGinty, R.K., Tan, S.H., (2014). Nucleosome, and chromatin structure. In: Workman, J.L., Abmayr, S.M. (Eds.), *Fundamentals of chromatin*. Springer, New York, New York, NY, pp. 1–28.
8. Lipfert, J., Doniach, S., Das, R., Herschlag, D., (2014). Understanding nucleic acid-ion interactions. *Annu. Rev. Biochem.* **83**, 813–841.
9. Onufriev, A.V., Schiessel, H., (2019). The nucleosome: from structure to function through physics. *Curr. Opin. Struct. Biol.* **56**, 119–130.

10. Marsden, M.P., Laemmli, U.K., (1979). Metaphase chromosome structure: evidence for a radial loop model. *Cell* **17**, 849–858.
11. Widom, J., Klug, A., (1985). Structure of the 300A chromatin filament: X-ray diffraction from oriented samples. *Cell* **43**, 207–213.
12. McGhee, J.D., Nickol, J.M., Felsenfeld, G., Rau, D.C., (1983). Higher order structure of chromatin: orientation of nucleosomes within the 30 nm chromatin solenoid is independent of species and spacer length. *Cell* **33**, 831–841.
13. Schalch, T., Duda, S., Sargent, D.F., Richmond, T.J., (2005). X-ray structure of a tetranucleosome and its implications for the chromatin fibre. *Nature* **436**, 138–141.
14. Dorigo, B., Schalch, T., Bystricky, K., Richmond, T.J., (2003). Chromatin fiber folding: requirement for the histone H4 N-terminal tail. *J. Mol. Biol.* **327**, 85–96.
15. Lobbia, V.R., Trueba Sanchez, M.C., van Ingen, H., (2021). Beyond the nucleosome: nucleosome-protein interactions and higher order chromatin structure. *J. Mol. Biol.* **433**, 166827
16. Korolev, N., Fan, Y., Lyubartsev, A.P., Nordenskiold, L., (2012). Modelling chromatin structure and dynamics: status and prospects. *Curr. Opin. Struct. Biol.* **22**, 151–159.
17. Lu, Q., Wallrath, L.L., Elgin, S.C., (1994). Nucleosome positioning and gene regulation. *J. Cell. Biochem.* **55**, 83–92.
18. Studitsky, V.M., Kassavetis, G.A., Geiduschek, E.P., Felsenfeld, G., (1997). Mechanism of transcription through the nucleosome by eukaryotic RNA polymerase. *Science* **278**, 1960–1963.
19. Polach, K.J., Widom, J., (1995). Mechanism of protein access to specific DNA sequences in chromatin: a dynamic equilibrium model for gene regulation. *J. Mol. Biol.* **254**, 130–149.
20. Polach, K.J., Widom, J., (1996). A model for the cooperative binding of eukaryotic regulatory proteins to nucleosomal target sites. *J. Mol. Biol.* **258**, 800–812.
21. Hodges, C., Bintu, L., Lubkowska, L., Kashlev, M., Bustamante, C., (2009). Nucleosomal fluctuations govern the transcription dynamics of RNA polymerase II. *Science* **325**, 626–628.
22. Jenuwein, T., Allis, C.D., (2001). Translating the histone code. *Science* **293**, 1074–1080.
23. Turner, B.M., (2002). Cellular memory and the histone code. *Cell* **111**, 285–291.
24. Becker, P.B., Workman, J.L., (2013). Nucleosome remodeling and epigenetics. *Cold Spring Harb. Perspect. Biol.* **5**
25. Zentner, G.E., Henikoff, S., (2013). Regulation of nucleosome dynamics by histone modifications. *Nature Struct. Mol. Biol.* **20**, 259–266.
26. Kouzarides, T., (2007). Chromatin modifications and their function. *Cell* **128**, 693–705.
27. Rivera, C.M., Ren, B., (2013). Mapping human epigenomes. *Cell* **155**, 39–55.
28. Agalioti, T., Chen, G., Thanos, D., (2002). Deciphering the transcriptional histone acetylation code for a human gene. *Cell* **111**, 381–392.
29. Berger, S.L., (2002). Histone modifications in transcriptional regulation. *Curr. Opin. Genet. Dev.* **12**, 142–148.
30. Blossey, R., Schiessel, H., (2018). The Latest Twists in Chromatin Remodeling. *Biophys. J.* **114**, 2255–2261.
31. Bowman, G.D., Poirier, M.G., (2015). Post-translational modifications of histones that influence nucleosome dynamics. *Chem. Rev.* **115**, 2274–2295.
32. Millan-Zambrano, G., Burton, A., Bannister, A.J., Schneider, R., (2022). Histone post-translational modifications - cause and consequence of genome function. *Nature Rev. Genet.* **23**, 563–580.
33. Shogren-Knaak, M. et al, (2006). Histone H4–K16 acetylation controls chromatin structure and protein interactions. *Science* **311**, 844–847.
34. Cosgrove, M.S., Boeke, J.D., Wolberger, C., (2004). Regulated nucleosome mobility and the histone code. *Nature Struct. Mol. Biol.* **11**, 1037–1043.
35. Neumann, H. et al, (2009). A method for genetically installing site-specific acetylation in recombinant histones defines the effects of H3 K56 acetylation. *Mol. Cell* **36**, 153–163.
36. Dion, M.F., Altschuler, S.J., Wu, L.F., Rando, O.J., (2005). Genomic characterization reveals a simple histone H4 acetylation code. *PNAS* **102**, 5501–5506.
37. Oliva, R., Bazett-Jones, D.P., Locklear, L., Dixon, G.H., (1990). Histone hyperacetylation can induce unfolding of the nucleosome core particle. *Nucleic Acids Res.* **18**, 2739–2747.
38. Shahbazian, M.D., Grunstein, M., (2007). Functions of site-specific histone acetylation and deacetylation. *Annu. Rev. Biochem* **76**, 75–100.
39. Wang, X., Hayes, J.J., (2008). Acetylation mimics within individual core histone tail domains indicate distinct roles in regulating the stability of higher-order chromatin structure. *Mol. Cell Biol.* **28**, 227–236.
40. Bedford, M.T., Clarke, S.G., (2009). Protein arginine methylation in mammals: who, what, and why. *Mol. Cell* **33**, 1–13.
41. Black, J.C., Van Rechem, C., Whetstine, J.R., (2012). Histone lysine methylation dynamics: establishment, regulation, and biological impact. *Mol. Cell* **48**, 491–507.
42. Lachner, M., O'Carroll, D., Rea, S., Mechtler, K., Jenuwein, T., (2001). Methylation of histone H3 lysine 9 creates a binding site for HP1 proteins. *Nature* **410**, 116–120.
43. Bannister, A.J. et al, (2001). Selective recognition of methylated lysine 9 on histone H3 by the HP1 chromo domain. *Nature* **410**, 120–124.
44. Plath, K. et al, (2003). Role of histone H3 lysine 27 methylation in X inactivation. *Science* **300**, 131–135.
45. Alekseyenko, A.A., Gorchakov, A.A., Kharchenko, P.V., Kuroda, M.I., (2014). Reciprocal interactions of human C10orf12 and C17orf96 with PRC2 revealed by BioTAP-XL cross-linking and affinity purification. *PNAS* **111**, 2488–2493.
46. Margueron, R., Reinberg, D., (2011). The Polycomb complex PRC2 and its mark in life. *Nature* **469**, 343–349.
47. Yuan, W. et al, (2012). Dense chromatin activates Polycomb repressive complex 2 to regulate H3 lysine 27 methylation. *Science* **337**, 971–975.
48. Bannister, A.J. et al, (2005). Spatial distribution of di- and tri-methyl lysine 36 of histone H3 at active genes. *J. Biol. Chem.* **280**, 17732–17736.
49. Vakoc, C.R., Sachdeva, M.M., Wang, H., Blobel, G.A., (2006). Profile of histone lysine methylation across

transcribed mammalian chromatin. *Mol. Cell Biol.* **26**, 9185–9195.
50. Sharda, A., Humphrey, T.C., (2022). The role of histone H3K36me3 writers, readers and erasers in maintaining genome stability. *DNA Repair (Amst)* **119**, 103407
51. Musselman, C.A. et al, (2012). Molecular basis for H3K36me3 recognition by the Tudor domain of PHF1. *Nature Struct. Mol. Biol.* **19**, 1266–1272.
52. Vezzoli, A. et al, (2010). Molecular basis of histone H3K36me3 recognition by the PWWP domain of Brpf1. *Nature Struct. Mol. Biol.* **17**, 617–619.
53. Ordu, O., Lusser, A., Dekker, N.H., (2016). Recent insights from in vitro single-molecule studies into nucleosome structure and dynamics. *Biophys. Rev.* **8**, 33–49.
54. Killian, J.L., Li, M., Sheinin, M.Y., Wang, M.D., (2012). Recent advances in single molecule studies of nucleosomes. *Curr. Opin. Struct. Biol.* **22**, 80–87.
55. Kaczmarczyk, A., Brouwer, T.B., Pham, C., Dekker, N.H., van Noort, J., (2018). Probing chromatin structure with magnetic tweezers. *Methods Mol. Biol.* **1814**, 297–323.
56. Mack, A.H., Schlingman, D.J., Ilagan, R.P., Regan, L., Mochrie, S.G., (2012). Kinetics and thermodynamics of phenotype: unwinding and rewinding the nucleosome. *J. Mol. Biol.* **423**, 687–701.
57. Diaz-Celis, C. et al, (2022). Assignment of structural transitions during mechanical unwrapping of nucleosomes and their disassembly products. *Proc. Natl. Acad. Sci. U. S. A.* **119**, e2206513119
58. Yodh, J.G., Lyubchenko, Y.L., Shlyakhtenko, L.S., Woodbury, N., Lohr, D., (1999). Evidence for nonrandom behavior in 208–12 subsaturated nucleosomal array populations analyzed by AFM. *Biochemistry* **38**, 15756–15763.
59. Davies, E., Teng, K.S., Conlan, R.S., Wilks, S.P., (2005). Ultra-high resolution imaging of DNA and nucleosomes using non-contact atomic force microscopy. *FEBS Lett.* **579**, 1702–1706.
60. Konrad, S.F. et al, (2021). High-throughput AFM analysis reveals unwrapping pathways of H3 and CENP-A nucleosomes. *Nanoscale* **13**, 5435–5447.
61. Konrad, S.F., Vanderlinden, W., Lipfert, J., (2022). Quantifying epigenetic modulation of nucleosome breathing by high-throughput AFM imaging. *Biophys. J.* **121**, 841–851.
62. Konrad, S.F., Vanderlinden, W., Lipfert, J., (2021). A High-throughput Pipeline to Determine DNA and Nucleosome Conformations by AFM Imaging. *Bio Protoc.* **11**, e4180.
63. Heenan, P.R., Perkins, T.T., (2019). Imaging DNA equilibrated onto mica in liquid using biochemically relevant deposition conditions. *ACS Nano* **13**, 4220–4229.
64. Kepert, J.F. et al, (2003). Conformation of reconstituted mononucleosomes and effect of linker histone H1 binding studied by scanning force microscopy. *Biophys. J.* **85**, 4012–4022.
65. Shlyakhtenko, L.S., Lushnikov, A.Y., Lyubchenko, Y.L., (2009). Dynamics of nucleosomes revealed by time-lapse atomic force microscopy. *Biochemistry* **48**, 7842–7848.
66. Melters, D.P., Neuman, K.C., Bentahar, R.S., Rakshit, T., Dalal, Y., (2023). Single molecule analysis of CENP-A chromatin by high-speed atomic force microscopy. *Elife* **12**
67. Cui, Y., Bustamante, C., (2000). Pulling a single chromatin fiber reveals the forces that maintain its higher-order structure. *PNAS* **97**, 127–132.
68. Bennink, M.L. et al, (2001). Unfolding individual nucleosomes by stretching single chromatin fibers with optical tweezers. *Nature Struct. Biol.* **8**, 606–610.
69. Spakman, D., King, G.A., Peterman, E.J.G., Wuite, G.J. L., (2020). Constructing arrays of nucleosome positioning sequences using Gibson Assembly for single-molecule studies. *Sci. Rep.* **10**, 9903.
70. Meijering, A.E.C. et al, (2022). Nonlinear mechanics of human mitotic chromosomes. *Nature* **605**, 545–550.
71. Meng, H., Andresen, K., van Noort, J., (2015). Quantitative analysis of single-molecule force spectroscopy on folded chromatin fibers. *Nucleic Acids Res.* **43**, 3578–3590.
72. Chien, F.T., van Noort, J., (2009). 10 years of tension on chromatin: results from single molecule force spectroscopy. *Curr. Pharm. Biotechnol.* **10**, 474–485.
73. Smith, S.B., Cui, Y., Bustamante, C., (1996). Overstretching B-DNA: the elastic response of individual double-stranded and single-stranded DNA molecules. *Science* **271**, 795–799.
74. Bustamante, C., Marko, J.F., Siggia, E.D., Smith, S., (1994). Entropic elasticity of lambda-phage DNA. *Science* **265**, 1599–1600.
75. Smith, S.B., Finzi, L., Bustamante, C., (1992). Direct mechanical measurements of the elasticity of single DNA molecules by using magnetic beads. *Science* **258**, 1122–1126.
76. Kriegel, F., Ermann, N., Lipfert, J., (2017). Probing the mechanical properties, conformational changes, and interactions of nucleic acids with magnetic tweezers. *J. Struct. Biol.* **197**, 26–36.
77. Lipfert, J., van Oene, M.M., Lee, M., Pedaci, F., Dekker, N.H., (2015). Torque spectroscopy for the study of rotary motion in biological systems. *Chem. Rev.* **115**, 1449–1474.
78. Meglio, A. et al, (2009). Single DNA/protein studies with magnetic traps. *Curr. Opin. Struct. Biol.* **19**, 615–622.
79. Vilfan, I.D., Lipfert, J., Koster, D.A., Lemay, S.G., Dekker, N.H., (2009). Magnetic tweezers for single-molecule experiments. In: Hinterdorfer, P., Oijen, A. (Eds.), *Handbook of single-molecule biophysics*. Springer US, New York, NY, pp. 371–395.
80. Strick, T.R., Allemand, J.F., Bensimon, D., Bensimon, A., Croquette, V., (1996). The elasticity of a single supercoiled DNA molecule. *Science* **271**, 1835–1837.
81. Solis, F.J., Bash, R., Yodh, J., Lindsay, S.M., Lohr, D., (2004). A statistical thermodynamic model applied to experimental AFM population and location data is able to quantify DNA-histone binding strength and internucleosomal interaction differences between acetylated and unacetylated nucleosomal arrays. *Biophys. J.* **87**, 3372–3387.
82. Geeven, G. et al, (2015). Local compartment changes and regulatory landscape alterations in histone H1-depleted cells. *Genome Biol.* **16**, 289.
83. Collepardo-Guevara, R. et al, (2015). Chromatin unfolding by epigenetic modifications explained by dramatic impairment of internucleosome interactions: a multiscale computational study. *J. Am. Chem. Soc.* **137**, 10205–10215.

84. Chang, L., Takada, S., (2016). Histone acetylation dependent energy landscapes in tri-nucleosome revealed by residue-resolved molecular simulations. *Sci. Rep.* **6**, 34441.
85. Funke, J.J. et al, (2016). Uncovering the forces between nucleosomes using DNA origami. *Sci. Adv.* **2**, e1600974
86. Lowary, P.T., Widom, J., (1998). New DNA sequence rules for high affinity binding to histone octamer and sequence-directed nucleosome positioning. *J. Mol. Biol.* **276**, 19–42.
87. Lin, Y.Y., Brouns, T., Kolbeck, P.J., Vanderlinden, W., Lipfert, J., (2023). High-yield ligation-free assembly of DNA constructs with nucleosome positioning sequence repeats for single-molecule manipulation assays. *J. Biol. Chem.* **299**, 104874
88. Strick, R., Strissel, P.L., Gavrilov, K., Levi-Setti, R., (2001). Cation-chromatin binding as shown by ion microscopy is essential for the structural integrity of chromosomes. *J. Cell Biol.* **155**, 899–910.
89. Thoma, F., Koller, T., Klug, A., (1979). Involvement of histone H1 in the organization of the nucleosome and of the salt-dependent superstructures of chromatin. *J. Cell Biol.* **83**, 403–427.
90. Allahverdi, A., Chen, Q., Korolev, N., Nordenskiold, L., (2015). Chromatin compaction under mixed salt conditions: opposite effects of sodium and potassium ions on nucleosome array folding. *Sci. Rep.* **5**, 8512.
91. Ohyama, T., (2019). New aspects of magnesium function: a key regulator in nucleosome self-assembly, chromatin folding and phase separation. *Int. J. Mol. Sci.* **20**
92. Schwarz, P.M., Felthauser, A., Fletcher, T.M., Hansen, J. C., (1996). Reversible oligonucleosome self-association: dependence on divalent cations and core histone tail domains. *Biochemistry* **35**, 4009–4015.
93. Gebala, M., Johnson, S.L., Narlikar, G.J., Herschlag, D., (2019). Ion counting demonstrates a high electrostatic field generated by the nucleosome. *Elife* **8**
94. Dwiranti, A. et al, (2014). The effect of magnesium ions on chromosome structure as observed by helium ion microscopy. *Microsc. Microanal.* **20**, 184–188.
95. Vizjak, P. et al, (2023). ISWI catalyzes nucleosome sliding in condensed nucleosome arrays. *bioRxiv*.
96. Engelhardt, M., (2004). Condensation of chromatin in situ by cation-dependent charge shielding and aggregation. *Biochem. Biophys. Res. Commun.* **324**, 1210–1214.
97. Valberg, L.S., Holt, J.M., Paulson, E., Szivek, J., (1965). Spectrochemical analysis of sodium, potassium, calcium, magnesium, copper, and zinc in normal human erythrocytes. *J. Clin. Invest.* **44**, 379–389.
98. Csernoch, L., Bernengo, J.C., Szentesi, P., Jacquemond, V., (1998). Measurements of intracellular Mg2+ concentration in mouse skeletal muscle fibers with the fluorescent indicator mag-indo-1. *Biophys. J.* **75**, 957–967.
99. Froschauer, E.M., Kolisek, M., Dieterich, F., Schweigel, M., Schweyen, R.J., (2004). Fluorescence measurements of free [Mg2+] by use of mag-fura 2 in Salmonella enterica. *FEMS Microbiol. Lett.* **237**, 49–55.
100. Brower-Toland, B.D. et al, (2002). Mechanical disruption of individual nucleosomes reveals a reversible multistage release of DNA. *PNAS* **99**, 1960–1965.
101. Mochrie, S.G. et al, (2013). Unwinding and rewinding the nucleosome inner turn: force dependence of the kinetic rate constants. *Phys. Rev. E Stat. Nonlin. Soft Matter Phys.* **87**, 012710
102. McCauley, M.J. et al, (2022). Human FACT subunits coordinate to catalyze both disassembly and reassembly of nucleosomes. *Cell Rep.* **41**, 111858
103. Claudet, C., Angelov, D., Bouvet, P., Dimitrov, S., Bednar, J., (2005). Histone octamer instability under single molecule experiment conditions. *J. Biol. Chem.* **280**, 19958–19965.
104. Mihardja, S., Spakowitz, A.J., Zhang, Y., Bustamante, C., (2006). Effect of force on mononucleosomal dynamics. *PNAS* **103**, 15871–15876.
105. Brower-Toland, B. et al, (2005). Specific contributions of histone tails and their acetylation to the mechanical stability of nucleosomes. *J. Mol. Biol.* **346**, 135–146.
106. Kruithof, M., van Noort, J., (2009). Hidden Markov analysis of nucleosome unwrapping under force. *Biophys. J.* **96**, 3708–3715.
107. Sheinin, M.Y., Li, M., Soltani, M., Luger, K., Wang, M.D., (2013). Torque modulates nucleosome stability and facilitates H2A/H2B dimer loss. *Nature Commun.* **4**, 2579.
108. Kim, S.H., Vlijm, R., van der Torre, J., Dalal, Y., Dekker, C., (2016). CENP-A and H3 nucleosomes display a similar stability to force-mediated disassembly. *PLoS One* **11**, e0165078
109. Bancaud, A. et al, (2006). Structural plasticity of single chromatin fibers revealed by torsional manipulation. *Nature Struct. Mol. Biol.* **13**, 444–450.
110. Kerssemakers, J.W.J. et al, (2006). Assembly dynamics of microtubules at molecular resolution. *Nature* **442**, 709–712.
111. Hall, M.A. et al, (2009). High-resolution dynamic mapping of histone-DNA interactions in a nucleosome. *Nature Struct. Mol. Biol.* **16**, 124–129.
112. Maeshima, K., Imai, R., Tamura, S., Nozaki, T., (2014). Chromatin as dynamic 10-nm fibers. *Chromosoma* **123**, 225–237.
113. Ricci, M.A., Manzo, C., Garcia-Parajo, M.F., Lakadamyali, M., Cosma, M.P., (2015). Chromatin fibers are formed by heterogeneous groups of nucleosomes in vivo. *Cell* **160**, 1145–1158.
114. Simon, M. et al, (2011). Histone fold modifications control nucleosome unwrapping and disassembly. *PNAS* **108**, 12711–12716.
115. Farr, S.E., Woods, E.J., Joseph, J.A., Garaizar, A., Collepardo-Guevara, R., (2021). Nucleosome plasticity is a critical element of chromatin liquid-liquid phase separation and multivalent nucleosome interactions. *Nature Commun.* **12**, 2883.
116. Tian, W. et al, (2019). The HRP3 PWWP domain recognizes the minor groove of double-stranded DNA and recruits HRP3 to chromatin. *Nucleic Acids Res.* **47**, 5436–5448.
117. Fei, J. et al, (2018). NDF, a nucleosome-destabilizing factor that facilitates transcription through nucleosomes. *Genes Dev.* **32**, 682–694.
118. Rona, G.B., Eleutherio, E.C.A., Pinheiro, A.S., (2016). PWWP domains and their modes of sensing DNA and histone methylated lysines. *Biophys. Rev.* **8**, 63–74.
119. Simpson, R.T., (1978). Structure of chromatin containing extensively acetylated H3 and H4. *Cell* **13**, 691–699.
120. Gibson, B.A. et al, (2019). Organization of Chromatin by Intrinsic and Regulated Phase Separation. *Cell* **179**, 470–484.e21.

121. Gilbert, N. et al, (2004). Chromatin architecture of the human genome: gene-rich domains are enriched in open chromatin fibers. *Cell* **118**, 555–566.
122. Bussiek, M., Mucke, N., Langowski, J., (2003). Polylysine-coated mica can be used to observe systematic changes in the supercoiled DNA conformation by scanning force microscopy in solution. *Nucleic Acids Res.* **31**, e137.
123. Vanderlinden, W., Lipfert, J., Demeulemeester, J., Debyser, Z., De Feyter, S., (2014). Structure, mechanics, and binding mode heterogeneity of LEDGF/p75-DNA nucleoprotein complexes revealed by scanning force microscopy. *Nanoscale* **6**, 4611–4619.
124. Walker, P.U., Vanderlinden, W., Lipfert, J., (2018). Dynamics and energy landscape of DNA plectoneme nucleation. *Phys. Rev. E* **98**, 042412
125. Lipfert, J., Hao, X., Dekker, N.H., (2009). Quantitative modeling and optimization of magnetic tweezers. *Biophys. J.* **96**, 5040–5049.
126. Cnossen, J.P., Dulin, D., Dekker, N.H., (2014). An optimized software framework for real-time, high-throughput tracking of spherical beads. *Rev. Sci. Instrum.* **85**, 103712
127. van Loenhout, M.T., Kerssemakers, J.W., De Vlaminck, I., Dekker, C., (2012). Non-bias-limited tracking of spherical particles, enabling nanometer resolution at low magnification. *Biophys. J.* **102**, 2362–2371.
128. Allan, D.W., (1966). Statistics of atomic frequency standards. *Proc. IEEE* **54**, 221–230.
129. van Oene, M.M. et al, (2018). Quantifying the precision of single-molecule torque and twist measurements using Allan Variance. *Biophys. J.* **114**, 1970–1979.
130. Czerwinski, F., Richardson, A.C., Oddershede, L.B., (2009). Quantifying noise in optical tweezers by Allan Variance. *Opt. Express* **17**, 13255–13269.
131. Lansdorp, B.M., Saleh, O.A., (2012). Power spectrum and Allan variance methods for calibrating single-molecule video-tracking instruments. *Rev. Sci. Instrum.* **83**, 025115
132. Eeftens, J.M., van der Torre, J., Burnham, D.R., Dekker, C., (2015). Copper-free click chemistry for attachment of biomolecules in magnetic tweezers. *BMC Biophys.* **8**, 9.